DOI: 10.1002/chem.200600545

Density Functional Embedded Cluster Study of Cu_4, Ag_4 and Au_4 Species Interacting with Oxygen Vacancies on the MgO(001) Surface

Konstantin M. Neyman,*[a] Chan Inntam,[b] Lyudmila V. Moskaleva,[b] and Notker Rösch*[b]

Abstract: Cu_4, Ag_4, and Au_4 species adsorbed on an MgO(001) surface that exhibits neutral (F_s) and charged (F_s^+) oxygen vacancies have been studied using a density functional approach and advanced embedding models. The gas-phase rhombic-planar structure of the coinage metal tetramers is only moderately affected by adsorption. In the most stable surface configuration, the plane of the tetramers is oriented perpendicular to the MgO(001) surface; one metal atom is attached to an oxygen vacancy and another one is bound to a nearby surface oxygen anion. A very similar structural motif was recently found on defect-free MgO(001), where two O^{2-} ions serve as adsorption sites. Following the trend of the interactions with the regular MgO(001) surface, Au_4 and Cu_4 bind substantially stronger to F_s and F_s^+ sites than Ag_4. This stronger adsorption interaction at oxygen vacancies, in particular at F_s, is partly due to a notable accumulation of electron density on the adsorbates. We also examined the propensity of small supported metal species to aggregate to adsorbed di-, tri- and tetramers. Furthermore, we demonstrated that core-level ionization potentials offer the possibility for detecting experimentally supported metal tetramers and characterizing them structurally with the help of calculated data.

Keywords: adsorption · density functional calculations · metal particles · structure and bonding

Introduction

Systems composed of metal particles or metal films supported on an oxide are of immediate relevance for many applications, one of which is heterogeneous catalysis.[1,2] For advancing this rapidly developing area, it is crucial to be able to characterize supported metal systems at the microscopic (atomic) level. However, such systems are rather complex and their formation is affected by many factors, which are difficult to control precisely under experimental conditions and which usually lead to a distribution of metal structures on oxides. Therefore, one rarely obtains sufficiently detailed and comprehensive microscopic information on metal/oxide interfaces from experiments alone. Nowadays, first-principles electronic structure calculations enable one to explore separately the factors governing formation and fate of films or nanoparticles, and to improve our understanding of metals supported on oxides on the basis of information complementary to experimental results.[3,4]

Several years ago we initiated systematic computational studies of small d-metal particles deposited on the touchstone oxide support MgO using density functional (DF) cluster models.[5] That early investigation was focused on the bonding of nine different single transition metal atoms to energetically favored O^{2-} sites of an ideal (unrelaxed) MgO(001) surface; a simple embedding of quantum mechanical (QM) cluster models in an array of point charges was employed to represent the electrostatic effect of an ionic substrate. In contrast to the rigid, practically unrelaxed regular (001) surface of MgO, many of the common oxide surfaces relax considerably; this relaxation has to be properly accounted for when one models adsorption complexes. Furthermore, there is experimental evidence that metal nucleation often preferentially occurs at defects rather than at regular sites of well-ordered terraces of oxide surfaces.[6–8] Among these sites, oxygen vacancies or color centers, neutral F_s (left after removal of an O atom) and charged F_s^+ (formed when an O^- anion is missing) are considered to

[a] Prof. K. M. Neyman
ICREA, 08010 Barcelona and Departament de Química Física
Universitat de Barcelona, 08028 Barcelona (Spain)
Fax: (+34) 93-402-21231
E-mail: konstantin.neyman@icrea.es

[b] Dr. C. Inntam, Dr. L. V. Moskaleva, Prof. N. Rösch
Technische Universität München, 85747 Garching (Germany)
Fax: (+49) 89-289-13622
E-mail: roesch@theochem.tu-muenchen.de

play a major role.[9] Relaxation effects may be very important for surfaces with defects.

Recently, we developed advanced tools for embedding cluster models in an elastic polarizable environment (EPE).[10,11] These methods allow one to describe accurately adsorption on metal-oxide surfaces of varying degrees of covalence while taking relaxation effects into account. We employed EPE embedding for ionic oxides to elucidate the adsorption of isolated Pd atoms on regular sites and oxygen vacancies of MgO(001).[10] We went on to apply the EPE method in a consistent fashion to investigate systematically the adsorption of 17 single d-metal atoms across the periodic table with the regular O^{2-} sites on MgO(001) terraces[12] as well as with F_s and F_s^+ oxygen vacancies.[13] These studies showed that, at variance with general belief, some d-metal atoms do not form stronger bound adsorption complexes with F-type surface defects than with regular sites and that metal atoms in M_1/F_s complexes accumulate considerable amount of electron density, which governs the trend of the adsorption energies. We also demonstrated that core level energies of adsorbed metal atoms are characteristic and that calculated values can help to detect experimentally and discriminate M_1/O^{2-}, M_1/F_s and M_1/F_s^+ complexes on MgO(001). We extended our studies of atoms on MgO(001) to larger metal particles employing the same computational approach, which is one of the most accurate cluster model methods currently available. For instance, we addressed interactions of coinage metal dimers and trimers with regular sites and O vacancies on MgO(001).[14]

In this article, we quantify structure and bonding of coinage monometallic tetramers M_4 (M = Cu, Ag, Au) adsorbed on F_s and F_s^+ defects of the MgO(001) surface and we analyze our results in light of recently studied M_4 adsorption complexes on regular sites.[15] In the following section we describe the substrate models employed to represent F_s and F_s^+ defects on MgO(001) terraces and provide computational details. Subsequently, we discuss the calculated geometric and bonding parameters of M_4 adsorption complexes on F_s and F_s^+ sites. Furthermore, motivated by experimental evidence that point defects on oxides may act as strong traps for metal particles,[7,8] we examine the propensity of adsorbed species M_1, M_2, M_3 to aggregate, forming di-, tri- and tetramers in the presence of F_s and F_s^+ defects on MgO(001). We also offer a way how the structures of adsorption complexes formed by small metal particles can be characterized with the help of calculated core-level ionization energies. The last section summarizes our results and provides an outlook.

Computational Details

The calculations were carried out at the all-electron level using the linear combination of Gaussian-type orbitals fitting-functions density functional (LCGTO-FF-DF) method[16] implemented in the parallel computer code PARAGAUSS.[17,18] We employed the gradient-corrected exchange-correlation functional BP86;[19,20] open-shell systems were described in spin-polarized fashion. In calculations involving 4d (Ag) and 5d atoms (Au), we used a scalar relativistic variant based on a second-order Douglas–Kroll transformation to decouple electronic and positronic degrees of freedom of the Dirac–Kohn–Sham equation.[21,22] The Gaussian-type atomic orbital basis sets, contracted in generalized fashion, were the same as in our previous studies:[12–15] Cu (15s11p6d) → [6s5p3d], Ag (18s13p9d) → [7s6p4d], Au (21s17p11d7f) → [9s8p6d4f], Mg (15s10p1d) → [6s5p1d], O (13s8p1d) → [6s5p1d]. The auxiliary basis sets, used in the LCGTO-FF-DF method to represent the electron charge density when treating the Hartree part of the electron-electron interaction, were constructed by properly scaling the s and p exponents of the orbital basis sets;[16] on each atom of the QM cluster, "polarization" exponents were added as geometric series with factors of 2.5, starting with 0.1 au for p and 0.2 au for d functions.[16] The resulting auxiliary basis sets were: Mg (15s,10r^2,5p,5d), O (13s,4r^2,5p,5d), Cu (15s,11r^2,5p,5d), Ag (18s,13r^2,5p,5d), Au (20s,17r^2,5p,5d).

The cluster models of the MgO substrate were embedded in an elastic polarizable environment (EPE).[10] A specially designed QM/molecular mechanical (MM) interface ensures a consistent description of the mutual influence of electronic and geometric changes that the QM cluster region and its environment undergo relative to the regular unperturbed surface.[10] We employed a $Mg_9O_8(Mg^{pp*})_{12}$ cluster as QM part of the system, modeling F_s and F_s^+ defect sites on the MgO(001) surface. Here, Mg^{pp*} labels pseudopotential centers Mg^{2+}, entirely without electrons, which saturate the coordination spheres of O anions at the cluster boundaries.[23] Our models feature C_s symmetry, which was exploited in the calculations.[24] Geometry optimizations of selected systems Cu_4/O^{2-}, Cu_4/F_s and Cu_4/F_s^+ completely without symmetry constraints revealed essentially unchanged structures and adsorption energies; normal mode analysis of C_1 models confirmed that the most stable complexes (structures A, see below) indeed correspond to local minima of the potential energy surfaces. To generate the environment of the QM part, we optimized a two-layer slab model of the MgO(001) surface at the classical MM level. Tests had shown[14] differences of only 1 pm for metal–MgO distances and 2 kJ mol^{-1} for binding energies compared to results of six-layer slab model.[12,13]

Adsorption energies, E_{ad}, were calculated with respect to the sum of the ground-state energy of a free metal species M_4 in its equilibrium geometry and the energy of the relaxed MgO(001) substrate with the defect site under study. The E_{ad} values were corrected for the basis set superposition error (BSSE), invoking the counterpoise method. To characterize the charge redistribution due to adsorption, we computed potential-derived charges (PDCs)[25] which reproduce the electrostatic potential in the area above the MgO (001) surface plane of the cluster models. The employed all-electron method enables one to calculate ionization potentials (IPs) of core levels and we did so for *ns* orbitals (with the principal quantum number $n = 3$ for Cu, 4 for Ag, and 5

for Au) of M_4 species adsorbed on MgO. To account for final-state effects, caused by electron relaxation in response to the formation of a core hole, we evaluated IPs as difference of (spin-polarized) total energies of the hole state Mns^{-1} and the ground state, at the equilibrium geometry of the latter. From tests with extended (more s exponents) and more flexible (uncontracted) orbital basis sets of the d-metal atoms we estimated relative IP values (IP shifts), calculated with the standard basis sets, to be accurate to 0.03 eV.

Results and Discussion

In the gas phase, the most stable structure of the tetramers Cu_4, Ag_4 and Au_4 is a planar rhombus (D_{2h}), with the M–M distances along the edges (239, 274 and 268 pm, respectively) close to those of the short diagonal (228, 262 and 263 pm, respectively); the alternative tetrahedral structures are computed 90–110 kJ mol^{-1} less stable.[15] The closed-shell ground states of the free tetramers are ~60 kJ mol^{-1} more stable than the corresponding triplet states. The atomization energy per atom of a Cu_4 rhombus, 146 kJ mol^{-1},[15] is larger than the corresponding atomization energies for Cu_3, 112 kJ mol^{-1}, and Cu_2, 102 kJ mol^{-1};[14] the same trend holds for Ag and Au analogues. The atomization energy of an Ag_4 rhombus was calculated at 107 kJ mol^{-1} per atom; the corresponding value for the Au_4 rhombus is 146 kJ mol^{-1} per atom, identical to the value obtained for Cu_4.[15] Thus, the first- (Cu) and third-row (Au) elements are substantially stronger bound as tetramers than the second-row element Ag; dimers and trimers of the coinage metals show the same trends of the binding energy.[14] Aside from the larger size of the silver atoms, this trend on going from Cu to Ag is due to a destabilization of the Ag 5s orbital compared to the Cu 4s orbital, which in Ag_4 largely eliminates the d–s orbital mixing that is substantial for Cu_4. For Au_4, the relativistic contraction of the Au 6s shell restores some s–d mixing and contributes to stronger M–M interactions between the gold atoms.[15,26]

For each coinage metal tetramer, we considered three different configurations on the MgO(001) surface: two upright structures, where the M_4 rhombus is attached to the substrate by two (Figure 1, mode A) or one atom M (mode B) and a moiety oriented parallel to the surface (mode C). In contrast to the lowest-energy structures A, structures B and C appear to be a local minimum only under C_{2v} symmetry constraints. In Tables 1–3, we collected calculated observables for the optimized adsorption complexes of M_4 on MgO(001), featuring either an F_s or F_s^+ defect. For easy comparison, we also present results of our previous calculations on M_4 moieties at regular O^{2-} sites of the MgO(001) surface.[15] Similarly to the metal tetramers on regular sites, all complexes with F_s sites, are closed-shell systems, whereas all M_4/F_s^+ moieties exhibit a doublet ground state.

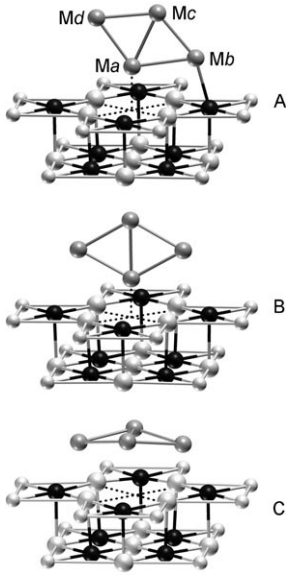

Figure 1. Sketches illustrating modes A, B, and C for adsorption complexes of Cu_4 at F_s vacancies of the MgO(001) surface. A: most stable structure at C_s symmetry constraints; B: model structure resulting from optimization under C_s symmetry constraints, started from a C_{2v} initial structure with vertically oriented Cu_4 species; C similar to B, but started from an initial structure with horizontally oriented Cu_4. Atom identifications: O (black), Mg (large white), Mg^{pp*} (small white), and Cu (light gray). For mode A, individual M atoms are labeled for easy identification (see text and tables). The shapes of Cu_4 complexes at F_s^+ sites as well as analogous complexes of Ag_4 and Au_4 are very similar.

Adsorption complexes of Cu_4: For Cu_4/F_s and Cu_4/F_s^+, the most stable structure among the complexes under scrutiny is the upright Cu_4 species mode A (see Table 1), with one Cu atom coordinated to a vacancy, F_s or F_s^+, and another Cu atom to a nearby O anion. A similar structure, but with two Cu_4–O bonds, was found to have the lowest energy for Cu_4 adsorbed on the defect-free surface MgO(001).[15] Even in that most strongly bound mode A of the Cu_4/F_s and Cu_4/F_s^+ systems, the rhombus Cu_4 is only moderately distorted upon adsorption. The largest structure change compared with the gas-phase tetramer[15] occurs on the edge *ab* (Figure 1) that is in direct contact with the surface, from 239 pm to 251 pm (F_s) or 243 pm (F_s^+). A similar elongation of the Cu–Cu bond (to 257 pm) has also been determined for the regular MgO(001) surface.[15] This bond lengthening (also observed for adsorbed Ag_4 and Au_4, Tables 2 and 3) is in line with the significant lattice mismatch between the interatomic distances within the MgO surface and the Cu (Ag, Au) particles: the shortest O–O distance in the substrate, 299 pm, is notably longer than the M–M distances in any of the coinage metal tetramers. The two bonds formed by each Cu_4 with the MgO terraces—to the O vacancy and the nearby O anion—are 168 and 209 pm, respectively, at F_s as well as 171 and 196 pm, respectively, at F_s^+. (For the first type of distance, the center of the defect is defined by averaging the coordinates of the four nearby Mg cations.) In the analogous structure A on the defect-free terraces, the Cu_4/O^{2-} complex exhibits two Cu–O bonds of slightly different length,

Table 1. Calculated properties[a] of surface complexes of Cu_4 species in three different adsorption modes on regular (O^{2-}) and oxygen vacancy (F_s, F_s^+) sites of MgO(001) terraces.

	Site[b]	Mode A[c]	Mode B	Mode C
r(Cu–Cu)	O^{2-}	257 *ab*, 232 *bc*, 243 *cd*, 235 *ad*, 234 *ac*	239 (4×), 229	247 (2×), 248 (2×), 227
	F_s	251 *ab*, 233 *bc*, 240 *cd*, 238 *ad*, 239 *ac*	238 (2×), 239 (2×), 237	241 (4×), 241
	F_s^+	243 *ab*, 232 *bc*, 238 *cd*, 234 *ad*, 258 *ac*	233 (2×), 251 (2×), 228	241 (4×), 237
∢Cu-Cu-Cu	O^{2-}	57, 58	57 (2×)	56 (2×)
	F_s	59, 60	60 (2×)	60 (2×)
	F_s^+	66 (2×)	56 (2×)	59 (2×)
r(Cu–O*)	O^{2-}	196 *a*, 205 *b*	190	279 (2×), 306, 312
	F_s	168 *a*, 209 *b*	141	222, 224, 260 (2×)
	F_s^+	171 *a*, 196 *b*	140	222 (2×), 276 (2×)
E_{ad}	O^{2-}	−191	−147	−84
	F_s	−305	−282	−272
	F_s^+	−220	−187	−194

[a] Distances in pm, angles in degree, energies in kJ mol^{-1}. r(Cu–O*): distance between the selected Cu centers and the nearest O^{2-} center or vacancy (the latter location defined as center of mass of its four Mg neighbors in the surface plane); E_{ad}: adsorption energy defined with respect to the sum of the ground-state energy of a free species Cu_4 in its equilibrium geometry and the energy of the relaxed substrate model cluster (negative values indicate exothermic adsorption). [b] Results for the M_4/O^{2-} complexes from ref. [15]. [c] In mode A, distances are identified by atom labels; see Figure 1.

196 pm to the central O of the Mg_9O_9 cluster and 205 pm to a nearby O anion.[15] The notably shorter contacts of adsorbates with F_s or F_s^+ vacancy sites than with O^{2-} sites mainly reflect the considerably reduced Pauli repulsion due to the missing O species, which no longer prevents metal particles from a closer approach to the surface. The adsorption energies of the complexes Cu_4/F_s and Cu_4/F_s^+ were calculated at −305 and −220 kJ mol^{-1}, respectively; these values are to be compared with −191 kJ mol^{-1} for the system Cu_4/O^{2-}.[15]

Using the hybrid B3LYP method, Del Vitto et al.[27] recently computed a similar geometry for Cu_4 adsorbed on an F_s center at the MgO(001) terrace. They obtained slightly longer Cu–Cu distances: 257 pm for the edge directly involved in the bonding with the surface, 246 pm for the opposite Cu–Cu edge. As in the present work, the angles Cu-Cu-Cu were around 60°. The corresponding adsorption energy, −333 kJ mol^{-1} (not corrected for BSSE), is slightly larger (by absolute value) than the present BP86 value of −305 kJ mol^{-1}, obtained after a BSSE correction of 26 kJ mol^{-1}.

Adsorption modes B, where Cu_4 is attached to a vacancy via a single Cu atom (Figure 1B), are 23 kJ mol^{-1} (F_s) and 33 kJ mol^{-1} (F_s^+) less stable than the corresponding mode A complexes (Table 1). For the complexes Cu_4/O^{2-} the bond weakening from A to B is slightly more pronounced, 44 kJ mol^{-1}.[15] Thus, a single bond of Cu_4 with the vacancy (or a central O^{2-} ion) in mode B already provides most of the adsorption interaction; the additional Cu_4–O^{2-} bond formed in mode A contributes only modestly to the overall stabilization, ~20% at regular O^{2-} sites and at most 10% at defect sites. In Cu_4/F_s (B), the distance between the center of the vacancy F_s and the nearest Cu atom (Cu–F_s) is 141 pm and the Cu–Cu distance perpendicular to the surface is 237 pm. This structure can be compared to the most stable, almost upright orientation of a Cu_2 moiety on an F_s site of MgO(001), with Cu–F_s and Cu–Cu distances at 170 and 233 pm, respectively.[14] In Cu_4/F_s^+ (B), the distance Cu–F_s^+ at 140 pm and the vertical distance Cu–Cu at 228 pm are in a similar correspondence with the values which we previously computed for Cu_2/F_s^+:[14] Cu–MgO 170 pm and Cu–Cu 230 pm. As in mode A, Cu_4 moieties in mode B are also able to come closer to the surface, when a vacancy is available for binding.

In mode C (Figure 1), Cu_4 is oriented essentially parallel to the surface with average heights of 214 pm (Cu_4/F_s) and 220 pm (Cu_4/F_s^+). Due to interactions with the substrate the planar adsorbate buckles somewhat. These structures exhibit significantly longer Cu–F_s or Cu–F_s^+ distances than in modes A and B: two Cu atoms form contacts with the O vacancy, at 260 pm (Cu_4/F_s) and 276 pm (Cu_4/F_s^+), whereas the other two Cu atoms are pair-wise bound to the next-nearest neighboring anions, at 222/224 pm (Cu_4/F_s) and 222 pm (Cu_4/F_s^+). The distances to the vacancies are substantially longer than in modes A or B, which is indicative of a weaker bonding with the vacancy. The limited bonding capacity of the vacancy is now shared over two Cu–F_s or Cu–F_s^+ bonds. Nevertheless, all favorable interactions with the substrate together bring the binding energy of mode C, −272 kJ mol^{-1} (Cu_4/F_s) and −194 kJ mol^{-1} (Cu_4/F_s^+), rather close to the corresponding values of mode B.

Adsorption complexes of Ag_4 and Au_4: The adsorption complexes of Ag_4 (Table 2) and Au_4 (Table 3) on oxygen defects of MgO(001) terraces are quite similar to the corresponding Cu_4 complexes discussed above in detail. For Ag_4, mode A is most stable, followed by modes B and C; the latter two exhibit essentially the same adsorption energies on F_s^+. This trend holds also for Au_4; the energetic preference of mode B compared with C is significant on F_s. Ag and Au atoms are larger than Cu, but not large enough to compensate the considerable mismatch between the nearest-neighbor O–O distance of the MgO(001) surface and optimum M–M distances in supported Ag_n and Au_n species.

Similar to single metal atoms,[5,10,12,13,28] dimers[14,28] and trimers[14,28] on the MgO(001) surface, Ag_4 tetramers form the weakest adsorption bonds among coinage metal congeners, not only with regular sites,[15] but also with color centers (Table 2). For the most stable adsorption modes A, one may compare the edge Ag–Ag distances in Ag_4/F_s at 265–283 pm and the short diagonal of the (pseudo-)rhombus Ag_4 at 281 pm to the analogous values of gas-phase Ag_4, 274

Table 2. Calculated properties of surface complexes of Ag_4 species in three different adsorption modes on regular (O^{2-}) and oxygen vacancy (F_s, F_s^+) sites of the MgO(001) terrace. All designations as in Table 1.

	Site	Mode A	Mode B	Mode C
r(Ag–Ag)	O^{2-}	288 *ab*, 264 *bc*, 281 *cd*, 268 *ad*, 268 *ac*	272 (2×), 276 (2×), 264	276 (4×), 269
	F_s	283 *ab*, 265 *bc*, 273 *cd*, 275 *ad*, 281 *ac*	272 (2×), 274 (2×), 278	272 (4×), 349
	F_s^+	275 *ab*, 271 *bc*, 267 *cd*, 283 *ad*, 278 *ac*	270 (2×), 277 (2×), 269	273 (4×), 283
∢Ag-Ag-Ag	O^{2-}	58 (2×)	58 (2×)	58 (2×)
	F_s	61, 62	61 (2×)	80 (2×)
	F_s^+	60, 61	59 (2×)	62 (2×)
r(Ag–O*)	O^{2-}	227 *a*, 232 *b*	225	275, 276 (3×)
	F_s	181 *a*, 237 *b*	158	274, 277, 298 (2×)
	F_s^+	186 *a*, 232 *b*	158	269, 270, 292 (2×)
E_{ad}	O^{2-}	−112	−96	−58
	F_s	−284	−276	−242
	F_s^+	−159	−148	−149

(edge) and 262 pm (diagonal).[15] The short diagonal is slightly increased compared with the gas-phase structure due to bonding competition between Ag–Ag and Ag–F_s bonds. Like Cu_4, Ag_4 binds via one atom to the central F_s vacancy and via another atom to a nearby O anion, resulting in bond lengths of 181 and 237 pm, respectively. The calculated adsorption energy is −284 kJ mol^{-1}. The Ag–Ag distances in Ag_4/F_s^+ (A), at 267–283 pm (edge) and 278 pm (diagonal), are similarly affected by adsorption as those in Ag_4/F_s. The Ag–F_s^+ bond, 186 pm, is only slightly longer (5 pm) than the corresponding bond with the neutral vacancy, despite that the adsorption energy of the former complex, −159 kJ mol^{-1}, is notably reduced with respect to Ag_4/F_s.

In mode B with an Ag_4 rhombus attached to the surface via a single Ag atom (Figure 1), adsorption to form the complexes Ag_4/F_s and Ag_4/F_s^+ is less exothermic than in mode A, but only by ~10 kJ mol^{-1}. The distances Ag–F_s and Ag–F_s^+, 158 pm, are considerably shorter, by 20 pm and more, compared with mode A. Similarly to adsorbed Cu_4, the single bonds Ag_4–F_s and Ag_4–F_s^+ in mode B already provide almost as much adsorbate–substrate stabilization as found in mode A, where an additional Ag_4–O^{2-} bond comes into play.

For Au_4 moieties, mode A is most stable (Table 3), with adsorption energies of −327 (Au_4/F_s^+) and −475 kJ mol^{-1} (Au_4/F_s). The latter complex exhibits the overall strongest adsorption interaction determined in the present study. The edge Au–Au distances in Au_4/F_s, 257–290 pm, scatter around the Au–Au values of Au_4 in the gas phase, 268 pm,[15] with the longest Au–Au distance, 290 pm, found between the atoms *a* and *b* directly attached to the substrate. Another notable adsorption-induced structural distortion of the Au_4 rhombus vs. the gas phase[15] is the elongation of its short diagonal from 263 to 284 pm. Considerably shorter bonds of adsorbed Au_4, both to the vacancy F_s, 160 pm, and to a nearby O anion, 228 pm, than in Ag_4/F_s clearly manifest a much stronger adsorption of the gold species. The same observation also holds for interactions with the charged defect F_s^+. In Au_4/F_s^+ (A), the longest Au–Au distance, 301 pm, is again that between the atoms in the immediate vicinity to the oxide. The other Au–Au edge distances, 258–272 pm, are even less affected by adsorption than those in Au_4/F_s. The Au–F_s^+ bond, 164 pm, is only 4 pm longer than the corresponding bond with the neutral vacancy, despite that the adsorption of the former complex, −327 kJ mol^{-1}, is destabilized compared to Au_4/F_s by as much as 148 kJ mol^{-1}. Interestingly, the bond Au_4–O^{2-} in the complex Au_4/F_s^+ (A) is shorter, 216 pm, than the Au_4–O^{2-} bonds, 220–222 pm, of Au_4/O^{2-} in mode A.[15] This geometric effect is reflected in the adsorption energy: mode B of Au_4/F_s^+ is notably less stable than mode A, by 68 kJ mol^{-1} (Table 3). The latter value indicates that the Au_4–O^{2-} bond of Au_4/F_s^+ (A) provides quite a significant stabilization in addition to the Au_4–F_s^+ bond, whereas in all other adsorption systems under scrutiny this stabilization is much smaller. Mode C of adsorbed Au_4 is less stable than modes A and B by 91 and 64 kJ mol^{-1} (Au_4/F_s) and by 95 and 27 kJ mol^{-1} (Au_4/F_s^+), respectively (Table 3).

Table 3. Calculated properties of surface complexes of Au_4 species in three different adsorption modes on regular (O^{2-}) and oxygen vacancy (F_s, F_s^+) sites of the MgO(001) terrace. All designations as in Table 1.

	Site	Mode A	Mode B	Mode C
r(Au–Au)	O^{2-}	301 *ab*, 256 *bc*, 272 *cd*, 260 *ad*, 278 *ac*	265 (2×), 277 (2×), 260	271 (4×), 269
	F_s	290 *ab*, 257 *bc*, 266 *cd*, 279 *ad*, 284 *ac*	265 (2×), 275 (2×), 277	269 (4×), 340
	F_s^+	301 *ab*, 272 *bc*, 271 *cd*, 258 *ad*, 279 *ac*	267 (2×), 269 (2×), 271	269 (4×), 282
∢Au-Au-Au	O^{2-}	59, 63	57 (2×)	60 (×2)
	F_s	62, 63	62 (2×)	78 (2×)
	F_s^+	58, 64	61 (2×)	63 (2×)
r(Au–O*)	O^{2-}	220 *a*, 222 *b*	216	277, 280, 294 (2×)
	F_s	160 *a*, 228 *b*	159	279, 281, 291 (2×)
	F_s^+	164 *a*, 216 *b*	161	274 (2×), 283 (2×)
E_{ad}	O^{2-}	−216	−158	−66
	F_s	−475	−448	−384
	F_s^+	−327	−259	−232

Electronic structure of small coinage metal species and their adsorption bonding: The results of the present study allow us to discuss the stability of small coinage metal particles of growing nuclearity on three different sites of MgO(001) surface. Previously we calculated that Cu_2, Ag_2 and Au_2 species (which are also closed-shell systems, like the tetramers considered here) exhibit notably stronger binding to oxygen vacancies, especially to F_s centers, than to regular O^{2-} sites.[14] All three tetramers display the same trend in adsorption

energy values E_{ad}, $M_4/F_s > M_4/F_s^+ > M_4/O^{2-}$ (Figure 2). Recently, we addressed the nature of adsorption interactions in M_4/O^{2-} systems on MgO(001).[15] Beyond the covalent contributions counteracted by Pauli repulsion, polarization

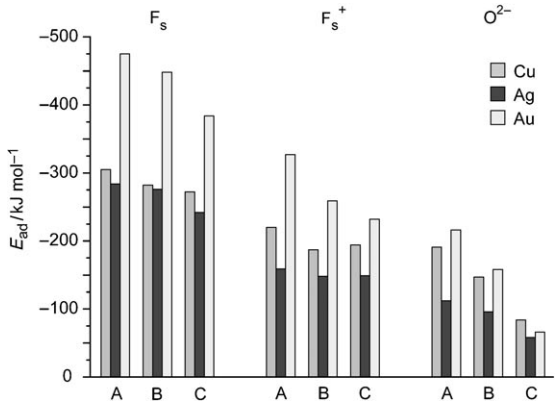

Figure 2. Comparison of adsorption energies calculated for various configurations of M_4 coinage metal species on regular sites and oxygen vacancies F_s and F_s^+ of a MgO(001) surface.

of the electronic shells of the metal species by the electrostatic field of the ionic substrate is important;[5] we interpreted the upright orientation of adsorbed M_4 as an indication of notable polarization effects.

The local electronic structure of the F_s center resembles that of a regular O^{2-} site in the sense, that the defect is formally saturated and has a very low electron affinity.[29] More specific "chemical" bonding contributions of M_4 to the F_s vacancy can be rationalized in a similar way as done for M_2 moieties:[14] the doubly occupied vacancy level (at ~2 eV above the valence band of the substrate) interacts with the lowest unoccupied orbital (LUMO) of the tetramers. The adsorption energies of the M_4 moieties at F_s sites are 1.6 (Cu_4), 2.5 (Ag_4) and 2.2 (Au_4) times larger (by absolute values) than at O^{2-} sites (Tables 1–3), very close to the corresponding ratios for the adsorbed dimers, 1.6, 2.7 and 2.4.[14] As for the adsorption of dimers, the trend $Au_4 > Cu_4 \geq Ag_4$ of the bonding interaction in M_4/F_s complexes correlates with the energies of the LUMO of the tetramers, which for Cu_4 and Ag_4 are 1.3 and 1.5 eV, respectively, below the vacancy level. Due to the relativistic stabilization of the Au 6s orbital,[26] the LUMO of Au_4 lies more than 2 eV lower. Thus, the adsorption energies of Cu_4 (-305 kJ mol^{-1}) and Ag_4 (-284 kJ mol^{-1}) at F_s defects are quite similar, whereas the bonding with Au_4 (-475 kJ mol^{-1}) is considerably stronger.

Another important stabilizing contribution to the binding in M_4/F_s complexes is due to a very pronounced transfer of electron density from the vacancy to the metal tetramers, which we quantified by PDC values $q(M_4)$ to almost a full electron charge (Table 4): -1.00, -0.99 and -0.97 e on Cu_4, Ag_4 and Au_4, respectively. (There is no contradiction between the anionic character of the adsorbed metal tetramers and their rather limited distortion with respect to the gas-phase structure because the bond lengths of free M_4 and M_4^- species are very close.[27]) These charges of the adsorbates are even larger by absolute value than those which we calculated for the dimers of the same metals, bound to F_s sites: -0.80, -0.83 and -0.73 e, respectively.[14] The difference seems to reflect the more limited capacity of smaller closed-shell metal entities to accommodate extra electron density. Indeed, the LUMOs of the metal dimers in the gas phase (which can be considered as a very rough guide for the electron affinity)[30] lie ~0.3 (Au) and ~0.5 eV (Cu, Ag) higher in energy than those of the corresponding tetramer species. In the adsorbed tetramers the accumulated electron density is preferentially transferred to the two metal atoms *a* and *b* (Figure 1A), which directly interact with the substrate: -0.72 e (Cu_4, Ag_4) and -0.62 e (Au_4). In contrast, the corresponding adsorbed metal dimers feature a more uniform charge distribution, with the charge on the M atom close to the substrate being -0.51, -0.52 and -0.36 e for Cu_2, Ag_2 and Au_2, respectively.[14] The M_4/F_s complexes have stronger adsorption bonds compared to their M_2/F_s analogues, by 91 (Cu), 70 (Ag) and 83 kJ mol^{-1} (Au). In addition to the discussed polar covalent bonding contributions, the adsorption of the tetramers relative to the dimers is strengthened due to an additional bond, M_4-O^{2-}, estimated as $E_{ad}(M_4/F_s, A) - E_{ad}(M_4/F_s, B)$ to contribute 23 (Cu), 8 (Ag) and 27 kJ mol^{-1} (Au). Finally, the larger polarizability

Table 4. Calculated potential-derived charges of (in e) and ionization potentials[a] (in eV) of atomic centers[b] of Cu_4, Ag_4 and Au_4 adsorbates on various sites of MgO(001) in the most stable structures A. Also shown are the corresponding averages of the ionization potentials over the adsorbate M_4.

	Charges					Ionization potentials				
	M*a*	M*b*	M*c*	M*d*	M_4	M*a*	M*b*	M*c*	M*d*	M_4
Cu_4/O^{2-}	−0.11	−0.38	0.01	−0.18	−0.66	115.7	115.5	115.4	115.1	115.4
Cu_4/F_s	−0.46	−0.26	−0.09	−0.19	−1.00	115.1	115.0	114.6	114.5	114.8
Cu_4/F_s^+	−0.57	−0.11	−0.04	0.08	−0.64	117.8	117.9	117.4	117.3	117.6
Ag_4/O^{2-}	0.05	−0.29	0.02	−0.15	−0.37	99.4	99.1	99.2	98.8	99.1
Ag_4/F_s	−0.33	−0.39	−0.06	−0.21	−0.99	98.9	98.6	98.3	98.2	98.5
Ag_4/F_s^+	−0.35	−0.13	0.02	−0.10	−0.56	101.4	101.1	100.9	100.6	101.0
Au_4/O^{2-}	−0.07	−0.34	−0.07	−0.14	−0.62	112.7	112.4	112.0	111.9	112.3
Au_4/F_s	−0.33	−0.29	−0.13	−0.22	-0.97	112.3	111.9	111.4	111.1	111.7
Au_4/F_s^+	−0.43	−0.12	−0.06	0.00	−0.61	114.6	114.8	114.0	113.8	114.3

[a] Ionization energies defined as the energy required for removing an electron from an *ns* level where $n = 3$, 4, 5 for M = Cu, Ag, Au, respectively. [b] For the labels M*i* of the various atomic centers of a complex of mode A, see Figure 1.

of the tetramers compared to the corresponding dimers also plays a role.

The electronic interaction in the adsorption complexes of the tetramers on a charged F_s^+ site is reminiscent of that taking place at an F_s vacancy. The adsorption interaction of each tetramer becomes weaker at the charged defect (Figure 2) as only one electron, instead of two in F_s, in the vacancy orbital is available for bonding. The binding $E_{ad}(M_4/F_s^+)$ in the M_4/F_s^+ systems is uniformly, by 30–40%, weaker than in the corresponding M_4/F_s complexes (Figure 2). In this way, the values $E_{ad}(M_4/F_s^+)$ are closer to the corresponding interaction energies $E_{ad}(M_4/O^{2-})$; for M = Cu and Ag, they are only ~30 or ~40 kJ mol^{-1} larger (by absolute value) than at O^{2-} sites. The trend $Au_4 > Cu_4 \geq Ag_4$ in the binding interaction of M_4/F_s complexes (see above) transforms insignificantly to $Au_4 > Cu_4 > Ag_4$ for the M_4/F_s^+ species. In fact, we identified very similar trends in the adsorption energies of the M_2/F_s^+ complexes among each other and with respect to their M_2/F_s analogues.[14]

As for M_4 adsorption complexes at neutral defects, one also finds transfer of electron density, initially located at the F_s^+ vacancy, to the adsorbed tetramers (Table 4). In line with the reduced occupancy of the vacancy level, these PDC values (Cu_4: −0.64 e, Ag_4: −0.56 e, Au_4: −0.61 e) are about 40% reduced compared to those calculated for adsorption complexes on neutral vacancies. The electron density transferred to M_4 particles from F_s^+ sites is essentially localized (~90% or more) on the two metal atoms closest to the oxide support (*a* and *b*, Figure 1A) and the larger part of this charge is on the atom M*a* directly bound to the vacancy. These results of the charge analysis for the M_4/F_s^+ species closely resemble the data we reported for adsorbed dimers in M_2/F_s^+;[14] however, the PDC values of the dimers are smaller by absolute value (Cu_2: −0.47 e; Ag_2, Au_2: −0.37 e). In fact, the total charges $q(M_4)$ of the adsorbates in the complexes M_4/F_s^+ are similar to those computed for adsorption at regular sites, M_4/O^{2-} (Table 4). In line with our findings for adsorption on F_s sites, the adsorption bonds in M_4/F_s^+ complexes are stronger than those in the M_2/F_s^+ moieties, by 88 (Cu), 31 (Ag) and 95 kJ mol^{-1} (Au).

Aggregation of small adsorbed metal species: We can estimate the propensity of deposited mono-, di- and triatomic species for coalescing to tetramers by combining energetic parameters calculated in the present work with the data for coinage metal particles supported on MgO from our previous systematic studies[12–15] which were all based on the same modeling strategy. In Table 5, we have collected the calculated reaction energies resulting for the agglomeration processes 1) $M_1 + M_1 \rightarrow M_2$, 2) $M_1 + M_2 \rightarrow M_3$, 3) $M_1 + M_3 \rightarrow M_4$, and 4) $M_2 + M_2 \rightarrow M_4$ on the three types of sites on the terraces of MgO(001). Results for the corresponding reactions in the gas phase were added as reference.

Table 5. Calculated energies [kJ mol^{-1}] of dimerization processes $M_m + M_n \rightarrow M_{m+n}$ of metal particles, $(m+n) \leq 4$, formed in the gas phase as well as on regular (O^{2-}) and defect (F_s, F_s^+) sites at MgO(001) terraces. Negative values correspond to exothermic processes.

M		Cu	Ag	Au
gas phase	(1) $M_1 + M_1 \rightarrow M_2$	−204[a]	−162[a]	−220[a]
	(2) $M_1 + M_2 \rightarrow M_3$	−131	−80	−128
	(3) $M_1 + M_3 \rightarrow M_4$	−246[b]	−186[b]	−235[b]
	(4) $M_2 + M_2 \rightarrow M_4$	−172[b]	−103[b]	−143[b]
regular O^{2-} sites	(1) $M_1/O^{2-} + M_1/O^{2-} \rightarrow M_2/O^{2-}$	−150[a]	−148[a]	−192[a]
	(2) $M_1/O^{2-} + M_2/O^{2-} \rightarrow M_3/O^{2-}$	−90	−60	−60
	(3) $M_3/O^{2-} + M_1/O^{2-} \rightarrow M_4/O^{2-}$	−163[b]	−146[b]	−164[b]
	(4) $M_2/O^{2-} + M_2/O^{2-} \rightarrow M_4/O^{2-}$	−103[b]	−56[b]	−32[b]
F_s defect	(1) $M_1/O^{2-} + M_1/F_s \rightarrow M_2/F_s$	−138[a]	−152[a]	−204[a]
	(3) $M_3/O^{2-} + M_1/F_s \rightarrow M_4/F_s$	−181	−186	−208
	(4) $M_2/O^{2-} + M_2/F_s \rightarrow M_4/F_s$	−135	−94	−63
F_s^+ defect	(1) $M_1/O^{2-} + M_1/F_s^+ \rightarrow M_2/F_s^+$	−2[a]	−16[a]	4[a]
	(3) $M_3/O^{2-} + M_1/F_s^+ \rightarrow M_4/F_s^+$	−43	−10	−13
	(4) $M_2/O^{2-} + M_2/F_s^+ \rightarrow M_4/F_s^+$	−132	−55	−75

[a] Ref. [14]. [b] Ref. [15].

Let us first consider the defect-free MgO(001) surface. There, combination of two dimers (reactions 4) is accompanied by energy gains of −103 (Cu), −56 (Ag), and −32 kJ mol^{-1} (Au).[15] These reactions are notably less exothermic than those of the corresponding metal species in the gas phase, −172, −103, and −143 kJ mol^{-1}.[15] Thus, the substrate counteracts sintering in a significant fashion, despite the fact that two adsorbed dimers, taken together, form the same number of M–O^{2-} bonds (two) as an adsorbed tetramer. In reactions 3, a change from two open-shell "reactants" M_1/O^{2-} and M_3/O^{2-} to a closed-shell "product" M_4/O^{2-} takes place. These transformations are more favorable than the dimerization of adsorbed dimers, although one M–O^{2-} bond is being lost. The corresponding energy gains for Cu, Ag and Au are −163, −146, and −164 kJ mol^{-1}.[15] The recombination (3) of a trimer with a single atom in the gas phase results in even higher energy gains of −246 (Cu), −186 (Ag) and −235 kJ mol^{-1} (Au), because pairing of electrons yields a strong bond between the two moieties without the expense of destabilizing a moderately strong bond with the support. When two open-shell atoms M form a closed-shell dimer, reactions 1, either in the gas phase or on regular MgO(001) sites,[14] the energies released are comparable to those of the other spin-quenching agglomeration of M_1 and M_3 (reactions 3, Table 5). The reaction energies of processes (1) are −150 (Cu), −148 (Ag) and −192 kJ mol^{-1} (Au) on the defect-free surface and −204 (Cu), −162 (Ag) and −220 kJ mol^{-1} (Au) for species in the gas phase.

One generally expects the very first elementary steps of metal particle growth to be significantly promoted in the

presence of defects. However, various DF results showed that the energetic preference of two atomic species to form homonuclear dimers (reactions 1) on isolated neutral F_s defect sites of the MgO(001) surface (Cu,[14,27,31] Ag,[14] Au,[14,32] Pd[33]) is not significantly larger or *even smaller* than that for the dimerization involving only regular MgO(001) sites (Table 5). For $M_1/O^{2-} + M_1/F_s$, we calculated reaction energies of −138 (Cu), −152 (Ag) and −204 kJ mol^{-1} (Au).[14] Furthermore, these reactions (1) on MgO(001) are essentially thermo-neutral for all three coinage metals, if charged defects F_s^+ are available for adsorption: $M_1/O^{2-} + M_1/F_s^+$ (Table 5).[14] Therefore, the formation of M_2 is strongly disfavored at F_s^+ sites compared with the same process on ideal MgO(001) terraces. This reflects the fact that open-shell monatomic Cu, Ag and Au moieties interact significantly stronger with open-shell F_s^+ sites than their closed-shell dimers.

How does this insight into the role of defects for the growth of small supported coinage metal particles carry over to the agglomeration leading to tetramers? To address this question, we calculated energies of reactions (3) and (4) on F_s and F_s^+ defect sites (Table 5). For each coinage metal, the formation of a tetramer on an F_s vacancy of MgO(001) from two adsorbed dimers is accompanied by an energy release which is uniformly larger, by ~30 kJ mol^{-1}, than that for the same reaction taking place on regular sites. Similarly, when the reactants are open-shell M_1 and M_3 moieties on MgO(001) forming M_4 products (reactions 4), the promotion effect of F_s sites with respect to the regular sites is 20–40 kJ mol^{-1} (Table 5). Thus, the propensity of F_s sites to facilitate agglomeration of coinage metal species into tetramers (reactions 3, 4) is not very large, but evident. This is in contrast to the above mentioned processes (1), where the formation of dimers on F_s sites was not favored compared with ideal MgO(001).

The presence of open-shell defects F_s^+ affects the thermodynamics of reactions 3 and 4 in a different way (Table 5). Aggregation of two (closed-shell) Cu or Au dimers (reactions 4) is 30–40 kJ mol^{-1} more favorable on an F_s^+ site than on the regular surface, while in the corresponding recombination of two Ag dimers on F_s^+ the same amount of energy is released as on the ideal MgO(001). However, dimerization of two open-shell moieties M_1 and M_3 (reactions 3) at an F_s^+ site shows only a very low exothermicity, much lower (by 120–150 kJ mol^{-1}) than on the regular surface (Table 5). This is in qualitative agreement with the results for the dimerization of open-shell atomic species M_1 (reactions 1) on F_s^+ defects. This latter reaction (1) has been predicted to be thermodynamically less favored than on the regular MgO(001) surface; it is even essentially thermoneutral.[14] In summary, whether or not F_s^+ defects on MgO(001) favor agglomeration of very small metal particles appears to depend on the spin state of the reactants and on their nuclearity. Based on the energies presented above, one may speculate that a probable scenario for the initial agglomeration steps of coinage metal particles in the presence of F_s^+ defects on MgO(001) could be similar to reactions 4: migration of a closed-shell metal fragment to another closed-shell metal species, attached at an F_s^+ site.

Core-level ionization potentials and valence density of states of adsorbed metal species: Finally, we address opportunities for monitoring the interaction of metal particles with regular and defect sites of metal oxide supports by means of X-ray photoelectron spectroscopy (XPS). Recently, a shift of the Au 4f XPS peak to lower binding energy, by −0.4 eV, has been detected for Au_1 species on TiO_2(110) at elevated temperatures and assigned to the migration of some Au atoms from regular sites to oxygen vacancies.[34] In response to these experiments, we theoretically quantified core-level energies of metal atoms deposited on MgO(001) and analyzed their dependence on the surface sites.[13] In that work we studied solely the initial-state effects and calculated shifts of Kohn–Sham core levels M*n*s for the complexes M_1/F_s and M_1/F_s^+ on MgO(001) relative to the corresponding values of the M_1/O^{2-} moieties. The core-level shifts of M_1 species were determined to be characteristic for the adsorption site. With the assumption that final-state effects, that is, relaxation of the final state in the presence of a core-level hole at M, are similar for M_1/O^{2-}, M_1/F_s^+ and M_1/F_s complexes of the same metal, diffusion of coinage metal atoms from regular O^{2-} to defect F_s sites has been calculated[13] to result in a negative M core-level shift (to lower binding energies), by −0.4 to −0.6 eV, in line with the experimental findings for the system Au_1/TiO_2(110).[34] In contrast, diffusion of M_1 moieties from O^{2-} to F_s^+ sites on MgO(001) was predicted to be manifested by positive core-level shifts.[13]

Here, we computed IP values for the M*n*s core levels of all individual atoms of nine adsorption complexes of the coinage metals M_4/MgO(001). However, we abandoned the previously employed initial-state approximation and explicitly accounted for electron relaxation effects that accompany the formation of a core hole. Thus, the IP values displayed in Table 4 were obtained as differences of spin-polarized total energy values of the core-hole state, Mns^{-1}, and the corresponding ground state, at the geometry of the latter. According to our test calculations on the IP values of Au 4f, which are often measured experimentally but are more demanding to calculate, computed Au 5s IPs represent shifts of the Au 4f levels with sufficient accuracy.

Analysis of the core ionization energies of the M_4/MgO complexes in Table 4 reveals trends similar to those found for the M_1/MgO systems with the initial-state approximation.[13] For instance, IP shifts of all M_4/F_s systems (where M_4 moieties bear a notable negative charge), both for individual atoms M and averages over M_4, are negative with respect to the corresponding reference values of M_4/O^{2-} and almost uniform for Cu, Ag and Au complexes. The average values $\Delta IP(M_4/F_s - M_4/O^{2-}) \equiv IP(M_4/F_s) - IP(M_4/O^{2-})$ for neutral defects are about −0.6 eV, indicative of XPS shifts of an experimentally detectable size. For all M_4/F_s^+ complexes under scrutiny, the corresponding XPS shifts are positive and even more pronounced than for the M_4/F_s analogues; $\Delta IP(M_4/F_s^+ - M_4/O^{2-})$ values range from 1.9 to 2.2 eV. [The

present results for XPS shifts based on IP(M_4/F_s^+) values were straightforward to obtain as differences of total energies, whereas uncertainties in shifts derived under the initial-state restrictions required special attention because of the charged character of the F_s^+ vacancy.[13]] IP values of specific atomic centers of adsorbed M_4 species scatter over ~0.6 eV for Cu_4 and Ag_4 and slightly more, from 0.8 to 1.2 eV, for Au_4 (Table 4). In almost all surface systems considered, atoms M*a*, interacting with the central site of the substrate cluster, feature a somewhat larger IP value than the corresponding atoms M*b*, attached to the nearby O^{2-} site. In turn, core electrons of atoms M*b* are stronger bound than in the atoms M*c* and M*d* of the same M_4 complex; the latter centers, forming the "upper" edge of the upright adsorbed M_4 moieties, are located farther from the oxide surface. Not unexpectedly, we did not find any clear correlation between the IP values (or their shifts) and the atomic charges (Table 4). Thus, extracting detailed and reliable information on the charge distribution from IP data has to be performed with due care.[35]

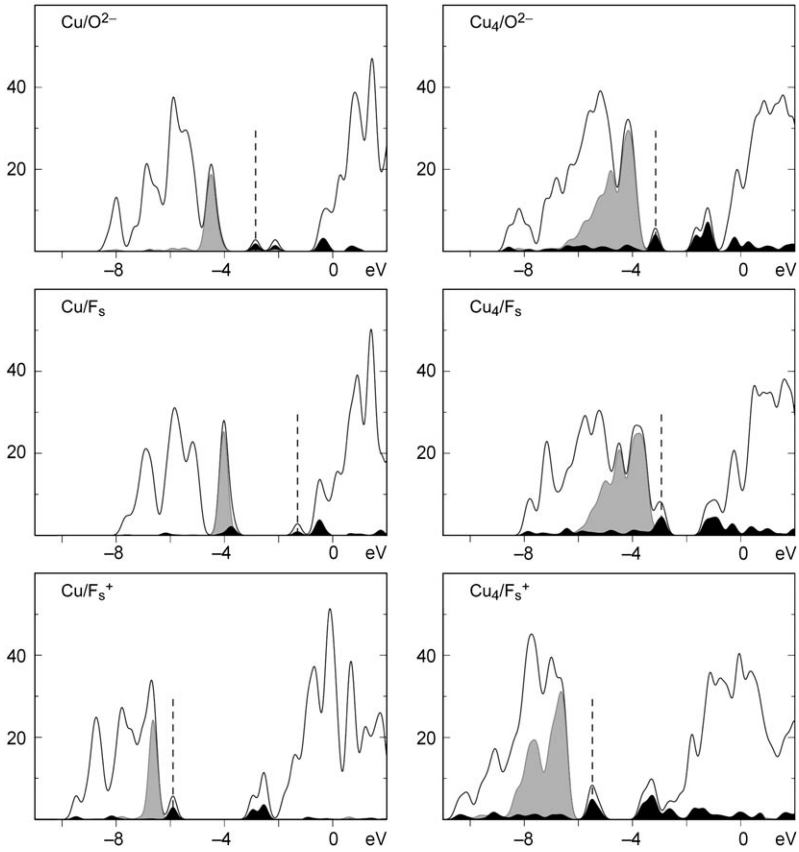

Figure 3. Calculated density of states (DOS) of surface complexes of Cu_1 and Cu_4 (mode A) species at regular sites (O^{2-}) and defects (F_s, F_s^+) of MgO(001) terrace. Besides the total DOS, the Cu d partial DOS (light shading) and the Cu s+p partial DOS (dark shading) are also shown. The position of the highest occupied Kohn–Sham level is marked by a vertical dashed line.

Obtaining sufficiently accurate structural details for small oxide-supported transition metal particles exclusively from experiment still remains a challenge.[36] Therefore, the above results are of particular importance. They show that calculated core-level ionization energies of individual atoms in the M_4 species on MgO (and thus also average values over M_4 complexes) are characteristic and, in combination with experimental XPS data, can open the way to distinguish between M_4/O^{2-}, M_4/F_s and M_4/F_s^+ structures on MgO(001) terraces.

In addition, experimentally accessible information on the energetic distribution of the valence levels, represented by calculated density of states (DOS) of supported metal species can be useful for detecting various complexes of small coinage metal particles. As an example, we present in Figure 3 DOS plots for Cu_1 and Cu_4 species on MgO(001). For both Cu_1 and Cu_4 species, the Cu 3d DOS structures on F_s sites are shifted slightly upward in energy (to less negative energies) with respect to the results for complexes at regular O^{2-} sites; on the other hand, the Cu 3d partial DOS is shifted downward on F_s^+ sites. This trend is in close agreement with the above discussion of calculated core-level IPs. Furthermore, one clearly sees how the structure of Cu 3d DOS develops (broadens) on each of the sites under study, when the metal moiety grows from an atom to a tetramer. Similar conclusions can be drawn from DOS plots of supported Ag_n and Au_n ($n = 1, 4$) on the three different adsorption sites on MgO(001) terraces (not shown).

Summary and Outlook

We studied tetramers of coinage metal atoms, Cu_4, Ag_4 and Au_4, deposited at neutral, F_s, and positively charged, F_s^+, oxygen vacancy sites of an MgO(001) terrace and we compared these results with those of analogous complexes at the regular, defect-free surface. For this purpose, we performed density functional calculations of cluster models, applying our recently developed approach of cluster embedding in an elastic polarizable environment.[10] All tetramers exhibit a distorted rhombus structure, favoring the same adsorption mode on both vacancy sites, where the adsorbed metal particles are oriented upright, perpendicular to the (001) surface, with one of their atoms bound to the defect and another one attached to a nearby surface oxygen anion. Similarly to dimer and trimer complexes of the coinage metals, Au_4 exhibits the strongest adsorption interaction on MgO(001) among all tetramers under scrutiny, followed by Cu_4 and Ag_4. The adsorption-induced distortions of the coinage metal particles are modest, reflecting that interactions

within the metal species are stronger than interactions with the support.

We quantified the propensity of very small supported metal particles to agglomerate to adsorbed di-, tri- and tetramers. At variance with a widespread belief, defects on MgO(001) terraces do not appear to stimulate the growth of these very small coinage metal clusters in a particularly strong fashion. Some coalescence processes on F_s^+, for example, attachment of M_1/O^{2-} or M_3/O^{2-} to M_1/F_s^+, are essentially energy-neutral. Calculated core-level ionization energies of individual atoms in MgO-supported metal tetramers revealed a characteristic dependence on the adsorption site and on the position within the adsorbate. In combination with experimental XPS data, these results open the way to distinguish between the M_4/O^{2-}, M_4/F_s and M_4/F_s^+ structures on MgO(001) terraces.

This work rounds off a series of our systematic theoretical studies of small MgO-supported transition metal particles, in particular, those formed by coinage metals.[10,12–15] A variety of data, obtained with the same accurate computational strategy, enabled us to quantify structural and binding parameters of adsorbed coinage metal particles and to draw some general conclusions which are expected to be applicable also to similar systems of other metals. For instance, we have shown that agglomeration (sintering) processes of the smallest metal species depend in a complicated way on the electronic state, nuclearity, and the type of adsorption site of the "reactant" and "product" complexes. Thus, the calculated results are crucial for quantifying and rationalizing these key phenomena of early phases of particle growth. Another finding of general importance is that core-level ionization potentials of small oxide-supported metal species seem sufficiently sensitive to the structure of the adsorption complexes, both to the local geometry of the metal subsystems and to the nature of the adsorption sites. Therefore, combination of measured XPS data with computational results appears to be a promising strategy for the structural characterization of supported metal particles.

Acknowledgements

NR thanks Professor F. Illas for his hospitality at the University of Barcelona where this work was cast into final form; financial support for a guest professorship has been provided by the Generalitat de Catalunya (PIV1-2005). This work was supported by Deutsche Forschungsgemeinschaft, Fonds der Chemischen Industrie (Germany), the Generalitat de Catalunya (2005SGR00697) and the Spanish Ministry of Education and Science (CTQ2005-08459-C02-01, UNBA05-33-001).

[1] G. A. Somorjai, *Introduction to Surface Chemistry and Catalysis*, Wiley, New York, **1994**.
[2] M. Bäumer, H.-J. Freund, *Prog. Surf. Sci.* **1999**, *61*, 127.
[3] *Chemisorption and Reactivity on Supported Clusters and Thin Films, NATO ASI Series E, Vol. 331* (Eds.: R. M. Lambert, G. Pacchioni), Kluwer, Dordrecht, **1997**.
[4] N. Rösch, V. A. Nasluzov, K. M. Neyman, G. Pacchioni, G. N. Vayssilov in *Computational Material Science, Theoretical and Computational Chemistry, Vol. 15* (Ed.: J. Leszczynski), Elsevier, Amsterdam, **2004**, p. 365.
[5] I. Yudanov, G. Pacchioni, K. Neyman, N. Rösch, *J. Phys. Chem. B* **1997**, *101*, 2786.
[6] I. Alstrup, P. J. Møller, *Appl. Surf. Sci.* **1988**, *33–34*, 143.
[7] M. Meunier, C. R. Henry, *Surf. Sci.* **1994**, *307–309*, 514.
[8] G. Haas, A. Menck, H. Brune, J. V. Barth, J. A. Venables, K. Kern, *Phys. Rev. B* **2000**, *61*, 11105.
[9] G. Pacchioni, *ChemPhysChem* **2003**, *4*, 1041.
[10] V. A. Nasluzov, V. V. Rivanenkov, A. B. Gordienko, K. M. Neyman, U. Birkenheuer, N. Rösch, *J. Chem. Phys.* **2001**, *115*, 8157.
[11] V. A. Nasluzov, E. A. Ivanova, A. M. Shor, G. N. Vayssilov, U. Birkenheuer, N. Rösch, *J. Phys. Chem. B* **2003**, *107*, 2228.
[12] K. M. Neyman, C. Inntam, V. A. Nasluzov, R. Kosarev, N. Rösch, *Appl. Phys. A* **2004**, *78*, 823.
[13] K. M. Neyman, C. Inntam, A. V. Matveev, V. A. Nasluzov, N. Rösch, *J. Am. Chem. Soc.* **2005**, *127*, 11652.
[14] C. Inntam, L. V. Moskaleva, K. M. Neyman, V. A. Nasluzov, N. Rösch, *Appl. Phys. A* **2006**, *82*, 181.
[15] C. Inntam, L. V. Moskaleva, I. V. Yudanov, K. M. Neyman, N. Rösch, *Chem. Phys. Lett.* **2006**, *417*, 515.
[16] B. I. Dunlap, N. Rösch, *Adv. Quantum Chem.* **1990**, *21*, 317.
[17] T. Belling, T. Grauschopf, S. Krüger, M. Mayer, F. Nörtemann, M. Staufer, C. Zenger, N. Rösch, in *High Performance Scientific and Engineering Computing, Lecture Notes in Computational Science and Engineering, Vol. 8* (Eds.: H.-J. Bungartz, F. Durst, C. Zenger), Springer, Heidelberg, **1999**, p. 439.
[18] T. Belling, T. Grauschopf, S. Krüger, F. Nörtemann, M. Staufer, M. Mayer, V. A. Nasluzov, U. Birkenheuer, A. Hu, A. V. Matveev, A. M. Shor, M. S. K. Fuchs-Rohr, K. M. Neyman, D. I. Ganyushin, T. Kerdcharoen, A. Woiterski, A. B. Gordienko, S. Majumder, N. Rösch, *ParaGauss*, Version 3.0, Technische Universität München, Munich, **2004**.
[19] A. D. Becke, *Phys. Rev. A* **1988**, *38*, 3098.
[20] J. P. Perdew, *Phys. Rev. B* **1986**, *33*, 8822; J. P. Perdew, *Phys. Rev. B* **1986**, *34*, 7406.
[21] O. D. Häberlen, N. Rösch, *Chem. Phys. Lett.* **1992**, *199*, 491.
[22] N. Rösch, A. Matveev, V. A. Nasluzov, K. M. Neyman, L. Moskaleva, S. Krüger in *Relativistic Electronic Structure Theory. Part II: Applications, Theoretical and Computational Chemistry Series, Vol. 14* (Ed.: P. Schwerdtfeger), Elsevier, Amsterdam, **2004**, p. 656.
[23] I. V. Yudanov, V. A. Nasluzov, K. M. Neyman, N. Rösch, *Int. J. Quantum Chem.* **1997**, *65*, 975.
[24] A. V. Matveev, M. Mayer, N. Rösch, *Comput. Phys. Commun.* **2004**, *160*, 91.
[25] B. H. Besler, K. M. Merz, P. A. Kollman, *J. Comput. Chem.* **1990**, *11*, 431.
[26] P. Pyykkö, *Chem. Rev.* **1988**, *88*, 563.
[27] A. Del Vitto, C. Sousa, F. Illas, G. Pacchioni, *J. Chem. Phys.* **2004**, *121*, 7457.
[28] G. Barbaro, A. Fortunelli, *J. Chem. Theory Comput.* **2005**, *1*, 972.
[29] A. V. Matveev, K. M. Neyman, I. V. Yudanov, N. Rösch, *Surf. Sci.* **1999**, *426*, 123.
[30] N. Rösch, S. B. Trickey, *J. Chem. Phys.* **1997**, *106*, 8940.
[31] A. Bogicevich, D. R. Jennison, *Surf. Sci.* **2002**, *515*, L481.
[32] A. Del Vitto, G. Pacchioni, F. Delbecq, P. Sautet, *J. Phys. Chem. B* **2005**, *109*, 8040.
[33] L. Giordano, C. Di Valentin, J. Goniakowski, G. Pacchioni, *Phys. Rev. Lett.* **2004**, *92*, 96105.
[34] S. Lee, C. Fan, T. Wu, S. L. Anderson, *Surf. Sci.* **2005**, *578*, 5.
[35] P. S. Bagus, F. Illas, G. Pacchioni, F. Parmigiani, *J. Electron Spectrosc. Relat. Phenom.* **1999**, *100*, 215.
[36] A. Hu, K. M. Neyman, M. Staufer, T. Belling, B. C. Gates, N. Rösch, *J. Am. Chem. Soc.* **1999**, *121*, 4522.

Received: April 17, 2006
Published online: September 13, 2006

